Hindawi
Journal of Nanomaterials
Volume 2023, Article ID 8812824, 10 pages
https://doi.org/10.1155/2023/8812824

Research Article

Hydroxyl Radical Generating Monovalent Copper Particles for Antimicrobial Application

Tze Hao Tan,[1] **Hao Zhang**,[1] **Bingqiao Xie**,[1] **Riti Mann**,[2] **Lingyi Peng**,[1] **Sung Lai Jimmy Yun**,[3] **Rose Amal**,[1] **Zi Gu**,[1] **and Cindy Gunawan**[2]

[1]*School of Chemical Engineering, UNSW Sydney, Sydney, NSW 2052, Australia*
[2]*Australian Institute for Microbiology and Infection, University of Technology Sydney, Ultimo, NSW 2007, Australia*
[3]*Qingdao International Academician Park Research Institute, Qingdao 266000, Shandong, China*

Correspondence should be addressed to Tze Hao Tan; tzehaotan@gmail.com, Zi Gu; zi.gu1@unsw.edu.au and Cindy Gunawan; cindy.gunawan@uts.edu.au

Received 17 January 2023; Revised 10 March 2023; Accepted 5 April 2023; Published 25 April 2023

Academic Editor: Jagpreet Singh

The antimicrobial properties of copper are well-known but maintaining a low oxidation state of Cu in particles is difficult. Herein, antimicrobial Cu_xP particles were synthesized through phosphorization of $Cu(OH)_2$, to lock copper in its monovalent state (as Cu_3P). We found that the phosphorization could be achieved at temperatures as low as 200°C, with stable surface presence of Cu(I) on the resulting Cu_xP particles. Cu(I) can act as a one-electron reducing agent for molecular oxygen, to generate the highly reactive hydroxyl radical. In this study, Cu_xP displayed antibacterial activities on the Gram-positive *Staphylococcus aureus* and Gram-negative *Escherichia coli*, with minimum inhibitory concentrations of 32 mg/L for the highest temperature particles (350°C) on both model bacteria. The evident membrane damage is consistent with the intended hydroxyl radical bacterial targeting mechanism. Low-temperature Cu_xP, although exhibiting lower antibacterial efficacies than those of the higher temperature variant, still showed competitive growth inhibiting activities when compared to other reported antimicrobial copper-based particles. The present work showcases advancements in particle technology that can lead to the development of a more robust antimicrobial agent, presenting a potent additive for self-disinfection applications.

1. Introduction

The world is now facing a pandemic-level infection, with pathogens capable of spreading via inanimate objects and surfaces. Research efforts have been increasingly focussed to address this so-called fomite transmission, in particular on the development of self-disinfecting materials. The application of antimicrobial agents on surfaces can reduce the risk of fomite transmission of pathogens in household and hospital settings, with the present work focusing on copper (Cu)-based antimicrobial particles. When compared to other metals, copper-based particles are cheaper to produce, with faster leaching rates, to release the toxic copper ions, including in biological systems [1–3]. Various copper-based antimicrobial particles have been developed, showing both *in vitro* and *in vivo* antibacterial activities [1]. For instance, metallic copper particles have been shown to exhibit bacterial-killing activities, with studies observing the particle apparent physical interactions with bacterial membranes, compromising their integrity [4]. Copper oxide (CuO) particles, on the other hand, have been indicated to exert different antibacterial mechanism, with the so-called Trojan horse-type toxicity. The mechanism involves intracellular leaching of copper ions following particle penetration into cells, leading to cell death and/or growth inhibition [4–7]. Copper-based particles have shown efficacies on Gram-positive and Gram-negative bacteria, both on their free-living planktonic and surface-attached biofilm forms of growth [4–7]. Research inquiries have further described the effects of particle characteristics on their antibacterial activities. Applerot et al. [5] found that smaller CuO particles (~2 nm) were associated with stimulation of a more intense oxidative stress, and therefore, a more effective antibacterial with higher extent of cell killing when compared to the larger particles (~30 nm). Studying the particle shapes, Laha et al. [8]

reported higher cell-killing effects of nanosized spherical CuO on Gram-negative bacteria (*Proteus vulgaris* and *Escherichia coli*), whereas nanosheets of CuO were more effective on Gram-positive bacteria (*Bacillus subtilis* and *Micrococcus luteous*).

Copper has also been combined with other metals to form antimicrobial alloys [9]. Zhou et al. [10] reported the cell-killing activities of Cu_2O–ZrP hybrid nanosheets on methicillin-resistant *Staphylococcus aureus* (MRSA) and vancomycin-resistant *Enterococcus*. The antibacterial effects were shown to correlate with the indicated oxygen radical targeting of bacterial membranes [10]. Likewise, Shalom et al. [7] reported the cell-killing activities of Zn-doped CuO nanoparticles (deposited on catheters) on urinary tract infection-causing bacterial pathogens (*E. coli*, *S. aureus*, and *P. mirabilis*). Combining Cu with silver has shown synergistic antibacterial effects; whereby presence of silver was indicated to increase the bacterial membrane permeability, increasing the growth inhibitory activities of the alloy to up to eight fold (on *E. coli* and *B. subtilis*), when compared to copper alone [11]. Metal ions have been indicated to interact with electronegative groups that are present in membrane phospholipids, with the interactions being linked, at least in part, to increasing membrane permeability and in turn, influx of the ions into bacteria to further disrupt cellular functions, including DNA synthesis [11]. A recent study by Tomina et al. [12] reported a significant increase in the antibacterial (on both Gram-positive and Gram-negative bacteria) and antifungal activities of mono- and bifunctional silica microspheres following doping with Cu(II), which are suggested to correlate with the oxygen radical-generating Fenton-like copper redox cycling (see below), leading to oxidative attack on membranes. Similarly, in a study by Naz et al. [13] Cu(II)-doped O-Carboxymethyl chitosan (OCMC) showed higher antibacterial activity on *E. coli* and *B. subtilis* in comparison to the OCMC alone. Another study by Wilks et al. [14] observed higher cell-killing rates (on *E. coli*) with increasing copper content in alloys with nickel, brass and steel, indicating major antimicrobial contribution from copper.

Copper antimicrobial applications, up to this stage, have explored the use of mainly Cu(II) and Cu(0)-based materials. For instance, quite recent work from our group found that a Cu(II) complex embedded within a poly(vinyl chloride) matrix could effectively inhibit the growth of surface-attached biofilms of nitrifying bacteria. The copper complex system generated nitric oxide, a quorum sensing inhibitor, *via* Cu(II)/Cu(I) redox cycling reactions when in the presence of nitrite and ascorbic acid (note that quorum sensing is a cell-to-cell communication signalling that allow controls of specific biological processes, including biofilm formation and adaptation to external stressors) [15]. Another example is a 3D printed Cu(0)-based self-disinfecting surfaces [16]. For the latter, a study by Champagne and Helfritch [3] demonstrated the cell-killing activities of three copper-based surfaces; developed by the deposition of Cu(0) using plasma spray, wire arc spray, and cold spray; on MRSA [3]. The cold spray technique, which results in the development of copper microstructure morphologies with enhanced diffusion of the toxic copper ions (more specifically, the high-velocity particle impact with the cold spray technique led to high grain dislocations density within the copper deposit, which in turn, increases copper ion diffusion in the metal), displayed the highest antibacterial activities [3]. Another study by Noyce et al. [17] observed a complete killing of MRSA suspensions (10^7 colony forming unit per mL) when exposed for 90 min at 22°C room temperature to Cu(0) surfaces. Although studies have reported the antimicrobial activities of Cu(I)-based materials [1, 2, 18–20], the use of Cu(I) however, is often hindered by its labile nature [15]. Cu(I)-containing antimicrobial systems have rarely been explored without an additional matrix support. Herein, the present work aims to develop a hydroxyl radical-generating antimicrobial copper particles, exploiting the relatively high redox potential of Cu(I). We synthesized Cu(I)-rich Cu_xP particles via facile phosphorization to help stabilize the surface presence of Cu(I) for a redox-based hydroxyl radical generation and studied their antimicrobial effects on model Gram-positive and Gram-negative bacteria. With a lower redox potential, Cu(I) species (Cu(I)/Cu(II) of 0.153 V) is more favorable than Cu(0) species (Cu(0)/Cu(II) of 0.342 V, Cu(0)/Cu(I) of 0.521 V) to induce the one-electron reduction of molecular oxygen (O_2) to form oxygen radicals [19]. The reactions generate superoxide radical $O_2^{\cdot-}$ from O_2 (non-Fenton, reaction 1). The $O_2^{\cdot-}$ then undergoes a proton-coupled electron transfer reaction to form H_2O_2 (Reaction 2), and ultimately, the Fenton-like reaction to form the highly reactive hydroxyl radical (Reaction 3) [21, 22].

Molecular oxygen reduction reactions:

$$O_2 + e^- \longrightarrow O_2^{\cdot-}, \quad (1)$$

$$O_2^{\cdot-} + e^- + 2H^+ \longrightarrow H_2O_2, \quad (2)$$

$$H_2O_2 + e^- \longrightarrow \cdot OH + OH^-. \quad (3)$$

Phosphorization of copper particles allows the locking of Cu in its monovalent state, potentially maintaining a high concentration of Cu(I) on the particle surface [23]. $Cu(OH)_2$ particles were first synthesized (by precipitation from a saturated ammonia solution), followed by phosphorization at different calcination temperatures. The phosphorization process led to the formation of Cu_3P (Cu(I) state) and CuP_2 (Cu(II) state), the latter more prevalent at higher calcination temperatures (≥300°C). Our study found that the Cu_xP particles exhibit competitive growth inhibiting activities when compared to other copper-based particles on the model bacteria. Further, we present studies elucidating the origins of the Cu_xP antibacterial activities, including the hydroxyl radical-mediated targeting.

2. Results

2.1. Synthesis and Characterisation of Cu_xP Particles. Phosphorization of $Cu(OH)_2$ was carried out in the presence of NaH_2PO_2 (under Ar atmosphere, NaH_2PO_2 decomposes to PH_3(g) at ≥200°C) at different calcination temperatures of 150–350°C to obtain CuO150, CuP200, CuP250, CuP300, and CuP350 particles. The extent of phosphorization was

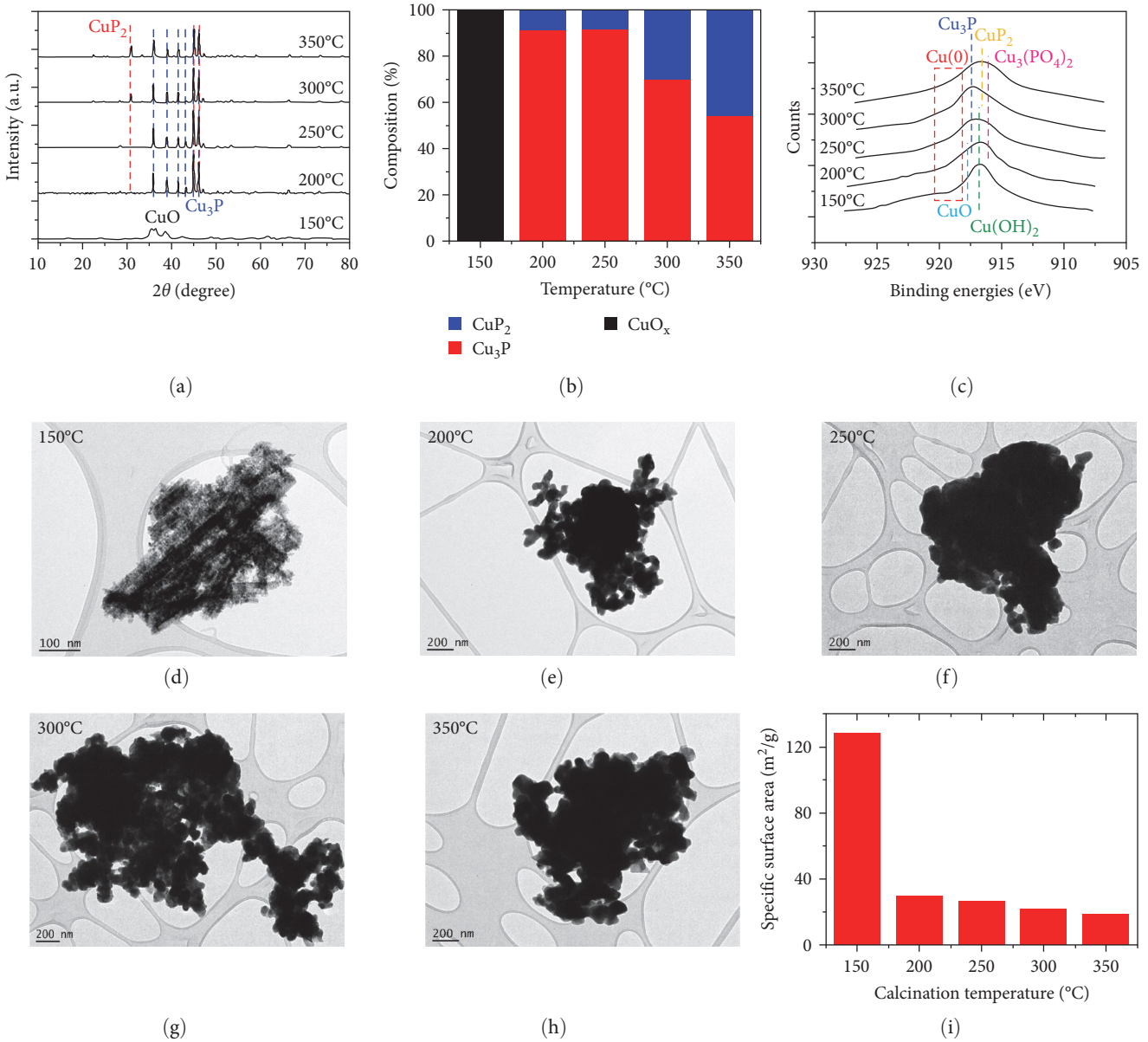

FIGURE 1: Crystal and chemical structure of CuO (150°C) and Cu_xP (200–350°C) particles at different calcination temperatures. (a, b) XRD spectra and bulk phase composition determined from the diffraction contribution of the identified phases, (c) XPS Cu LMM spectra identifying the surface composition, (dh) TEM images, and (i) BET-specific surface area.

examined with X-ray diffraction (XRD, Figure 1(a)). The XRD patterns of the calcined particles showed gradual shifts in chemical composition with increasing temperatures. At 150°C, the samples existed as CuO and Cu_2O, suggesting the dehydration and partial reduction of $Cu(OH)_2$. The oxides formation most likely resulted from direct redox reaction of $Cu(OH)_2$ with NaH_2PO_2, as the calcination temperature (150°C) was not sufficiently high for the NaH_2PO_2-to-PH_3 decomposition. At 200 and 250°C, the CuO and Cu_2O transformed to Cu_3P (Cu(I) state), along with CuP_2, the latter in small amounts (Figure 1(b)). The eutectic formation of CuP_2 became significant at ≥300°C (eutectic formation herein refers to the formation of CuP_2 as part of a solid-solution phase change of Cu_3P/CuP_2 mixture), with 30% of the calcined particles present as CuP_2 at 300°C, and ~45% at 350°C. It is worth noting that the formation of CuP_2 (Cu(II) state) is undesirable as it cannot act as a reducing agent for the intended formation of oxygen radicals.

Using X-ray photoelectron spectroscopy (XPS), we next analyzed the chemical states of Cu of the prepared particles (6 months after synthesis). The particle surface analysis was to also assess for the stable presence of the redox-active Cu(I) species. The Cu LMM spectra of the calcined particles (Figure 1(c)) showed shifts in the binding energies of the peaks with increasing temperatures, corresponding to the complex transitions of $Cu(OH)_2$ to CuO, Cu_3P, and CuP_2 (as well as $Cu_3(PO_4)_2$) (identified according to the work of Biesinger [24]). The presence of Cu LMM peak at 919.2 eV for CuO150

Table 1: Average hydrodynamic sizes, polydispersity index, and zeta potentials of CuO (150°C) and Cu_xP (200–350°C) particles in different media.

Sample	Average size (nm)	Polydispersity index	Zeta potential (mV)[a]
CuO150	114	0.65	–
CuP200	369	0.42	−20.8
CuP250	451	0.49	−27.1
CuP300	341	0.53	−22.0
CuP350	517	0.6	−22.6
PBS[b]	2,158	0.29	–
Tris–HCl[b]	1,197	0.31	−9.6

[a]Zeta potentials were measured in phosphate-buffered saline (PBS at pH 6), [b]CuP300 was dispersed in PBS or tris–HCl for hydrodynamic size, polydispersity index, and zeta potential measurements.

corresponds the surface presence of CuO, whereas the peaks at 917.6 eV for CuP200 to CuP350 calcined particles most likely correspond to the surface presence of the Cu(I) state Cu_3P species (Figure 1(c)). Note that no zero-valent Cu peak was seen in the Cu LMM spectra of the CuP200 to CuP350 particles, which indicates that the occurrence of Cu 2p peaks at 932.8 eV for the particles correspond solely to Cu(I) state (Figure S1). The observations indicate stable Cu(I) surface presence in these particles. For the higher temperature CuP300 and CuP350 calcined particles, the Cu LMM peaks at 916.5 eV most likely correspond to the surface presence of CuP_2 species (Figure 1(c)), which is consistent with the occurrence of the Cu(II) state peaks at 934.7 eV with the Cu 2p spectra (Figure S1). The (surface) detection of Cu_3P and CuP_2 are consistent with the appearance of symmetric P 2p peaks at 129.5 eV and 133.3 eV for the CuP200 to CuP350 particles (Figure S2). Further analysis also showed that a fraction of the (surface) Cu(II) species was present as $Cu_3(PO_4)_2$ for the CuP350 particle, as indicated by the occurrence of asymmetric P 2p peaks at 133.7 eV and 129.8 eV (Figure S2e). Also note that at lower calcination temperatures (≤250°C), some of the (surface) Cu was still present as $Cu(OH)_2$, as indicated by the presence of O 1 s peak at 533.1 eV (Figure S3).

To further understand the phosphorization process, we examined the particle size, morphologies, and aggregation. The electron transmission micrographs of CuO150 (with bulk composition of CuO, Cu_2O as well as $Cu(OH)_2$) showed spherical particles of <10 nm primary size (Figure 1(d)). Following the calcination at higher temperatures (≥200°C), sintering of the particles occurred with significant (∼100 nm increments) increase in primary size, with the elevated temperatures, with the particles no longer retaining the spherical morphologies (the sintering was a result of reaction between CuO and $PH_{3(g)}$, the latter was from NaH_2PO_2 decomposition). The measured surface area corroborated with the TEM micrographs of the particles (Figure 1(i)). The specific surface area of CuO150 was determined at 129 m^2/g, and after phosphorization, gradually decreasing to 30 m^2/g with the increasing temperatures (CuP200 to CuP350). The phosphorization, however, only caused minimal change in the particle "overall" aggregate size, with the increasing temperatures. The CuP200 to CuP350 particles (with bulk composition of mainly Cu_3P and CuP_2) fused, forming large aggregates (1,000–2,000 nm, Figure 1(e)–1(h)). Next, the hydrodynamic size of the calcined particles was studied via dynamic light scattering (DLS). As shown in Table 1, the average sizes of the particles are all within ∼350–550 nm range (excluding CuO150 with ∼100 nm size) when dispersed in water, with polydispersity indexes of 0.40–0.65. Again, we observed no significant impact of the calcination temperature on the hydrodynamic aggregate sizes. The colloidal stability of the CuP300 was further examined in PBS or tris–HCl, the latter used for the antibacterial studies. The average hydrodynamic sizes of CuP300 increased to 2.2 μm and 1.2 μm, respectively, in PBS and tris–HCl, indicating further aggregation and wider size distribution (0.29 (PBS) and 0.31 (tris–HCl) polydispersity index) in the buffer solutions, when compared to the water system. The aggregation was most likely attributed to the presence of relatively high concentrations of anions and counter cations in the buffer solutions, creating a charge shielding effect which neutralises long-range electrostatic interactions, in turn facilitating inter-particle interactions [25]. Smaller CuP300 aggregates were also likely to form in the tris–HCl system (relative to those in the PBS), due to the steric hindrance effects imposed by adsorbed tris molecules [26]. The zeta potential measurement showed a net negative surface charge of the Cu_xP (CuP200 to CuP350) particles in PBS (−20.8 to −27.1 mV). The different calcination temperatures did not seem to affect the zeta potential.

2.2. Oxygen Radical Formation by Cu_xP Particles. The coumarin test was used to assess the hydroxyl radical (·OH) generation of the CuO150 and Cu_xP (CuP200, CuP250, CuP300, CuP350) particles. Coumarin reacts with ·OH to form the fluorescent 7-OH-coumarin (450 nm) [27]. As shown in Figure 2(a), the CuO150 particle did not generate ·OH radicals, with essentially no detection of the fluorescence signal. This is consistent with the XRD and XPS data for CuO150 (Figure 1), showing that the particle is entirely composed of CuO, Cu_2O (and $Cu(OH)_2$), with no surface presence of Cu(I) species. The Cu_xP (Cu_3P and CuP_2) particles CuP200, CuP250, and CuP300 generated ·OH radicals, and at comparable extent, as shown by the overlapping 7-OH-coumarin fluorescence intensity detected over time (Figure 2(a)). The observations are in line with the similar ∼50% surface Cu(I) molar ratios (relative to Cu(II)) being estimated for CuP200, CuP250, and CuP300 from the XPS Cu 2p spectra (Figure 2(b), Figure S1). The surface Cu(I) molar ratio decreased to 30% for CuP350. Interestingly, the coumarin

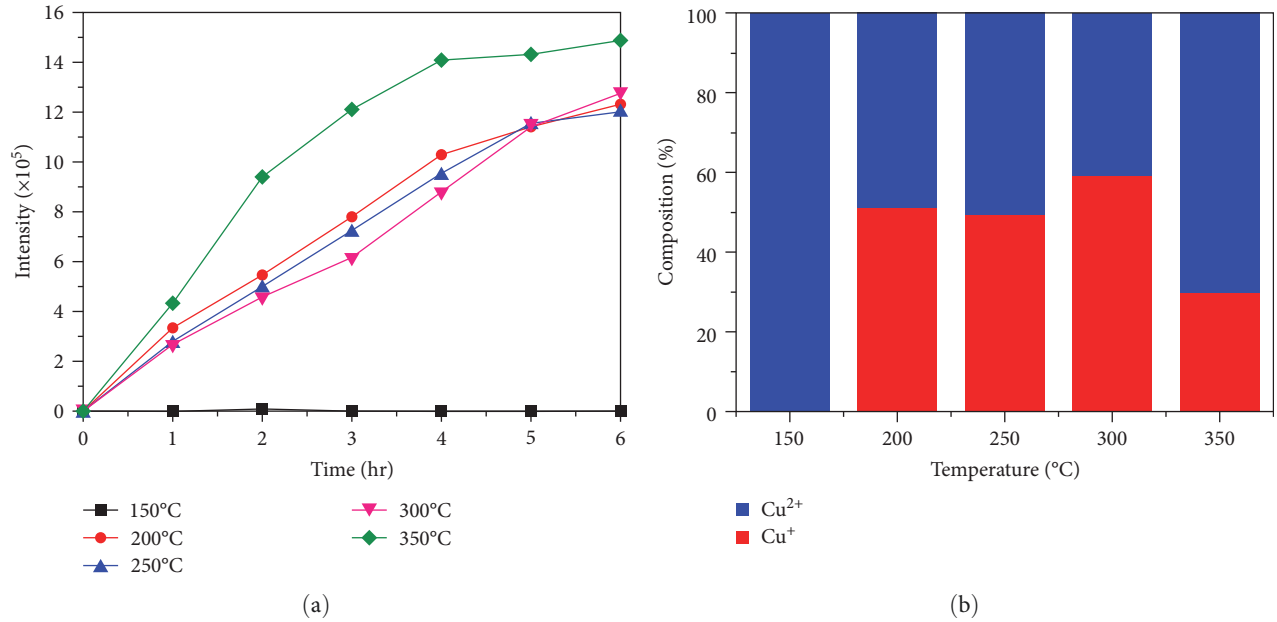

FIGURE 2: (a) Fluorescence signal intensity of 7-OH-coumarin (450 nm) for CuO (150°C) and Cu_xP (200–350°C) particles and (b) surface Cu states molar ratios determined from Cu 2p XPS spectra (Figure S1).

response for CuP350 was apparently the highest when compared to the lower temperature Cu_xP particles, indicating the most extensive ·OH generation. It is still unclear at this stage however, as with the underlying reasons for the highest extent of the radical generation for the CuP350 particles.

2.3. Antibacterial Efficacies of Cu_xP Particles and Mechanistic Studies. The antibacterial effects of the CuO and Cu_xP particles (CuO150, CuP200, 250, 300, 350) were assessed on a Gram-positive model bacterium *S. aureus* and a Gram-negative model bacterium *E. coli*. As shown in Figure 3, all the CuO and Cu_xP particles exhibited dose-dependent toxicity on *S. aureus* and *E. coli*. For example, exposures of *S. aureus* to increasing 8–256 mg/L CuP200 concentrations inhibited the growth of the bacterium, from ~80% extent of biomass growth (relative to the cell-only control growth) at 8 mg/L particle exposure to ~20% growth at 32 mg/L particle concentration, then ultimately to <5% growth at 256 mg/L concentration. Comparable trends were observed with *E. coli*, with ~95% growth at 8 mg/L CuP200 exposure to <5% growth at 256 mg/L particle concentration. Among the particles, CuP350 showed the highest growth inhibition effects with minimum inhibitory concentration (MIC, for ≥95% growth inhibition) of 32 mg/L for both *S. aureus* and *E. coli*, whereas CuO150 showed the lowest effects (MIC of >256 mg/L) (Figure 3). For CuP200, CuP250, and CuP300, the MICs were determined at 64 mg/L for both *S. aureus* and *E. coli*. These CuO and Cu_xP MICs are lower when compared to the previously studied copper-based antibacterial particles, although the much larger sizes of the particles (~100–2000 nm CuO and Cu_xP aggregates, Figure 1(d)1(i), Table 1). Sharma and Kumar [28] reported an MIC of 391 mg/L with CuO particles (d = 5–9 nm) on *E. coli*, whereas Gunawan et al. [29] reported a significantly higher CuO MIC of 900 mg/L (d = 14 nm) on *E. coli*. In another study, Argueta-Figueroa et al. [30] reported a 100 mg/L MIC with metallic Cu^0 particles (d = 4 nm) on *S. aureus* and *E. coli*. The apparent higher extent of growth-inhibiting activity observed in the present study is thought to result, at least in part, from the unique antibacterial mechanisms of the particles, as next described.

The antibacterial activities of our copper particles are most likely to primarily originate from the earlier described redox generation of hydroxyl radical (·OH). The levels of the growth-inhibiting activities are consistent with the extent of the radical generation. CuP350 with the lowest MICs (32 mg/L) on *S. aureus* and *E. coli*, produced the highest amount of ·OH radical, followed by CuP200, CuP250, and CuP300 with less ·OH formation and evidently, higher MICs (64 mg/L) on the bacteria (Figures 2(a) and 3). CuO150 with undetectable ·OH formation seemed to only "reach" MICs for both bacteria at >256 mg/L concentration. Hydroxyl radical is the most reactive oxygen radical, with research inquiries already establishing its reactivity on biomolecules. The one-electron oxidant has been known to cause peroxidation of phospholipids in bacterial cell envelopes (present in the inner membrane of *S. aureus*, and in the outer and inner membranes of *E. coli*) [31]. Initiated by abstraction of an allylic hydrogen atom, the peroxidation modifies lipids into lipid hydroperoxides. The radical can also cleave phosphate esters in phospholipids [31, 32]. These radical attacks on phospholipids, in many cases, have been known to result in leaky membranes [33, 34]. Herein, we stained the particle-exposed *E. coli* samples with AM1-43 fluorescent dye to probe the cell membranes phospholipid moieties [35, 36]. Indeed, leaky membranes were observed in the *E. coli* population for all tested particles (Figure 4). Note the less fluorescent (green) membranes of the particle-exposed bacterial samples when

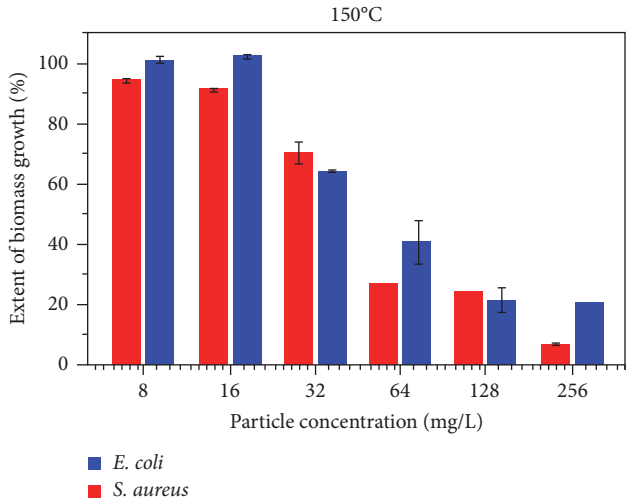

(a)

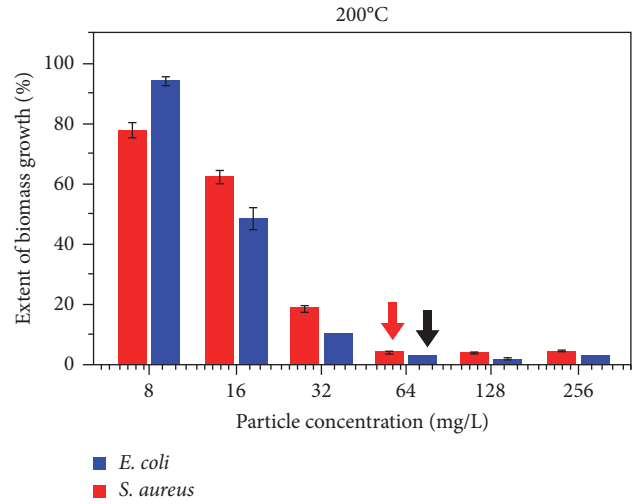

(b)

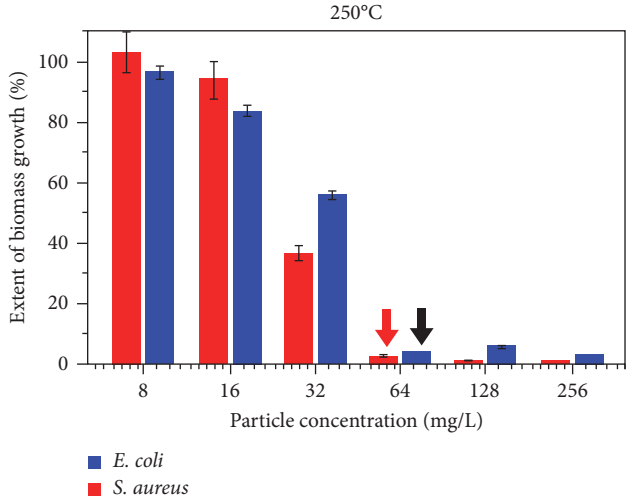

(c)

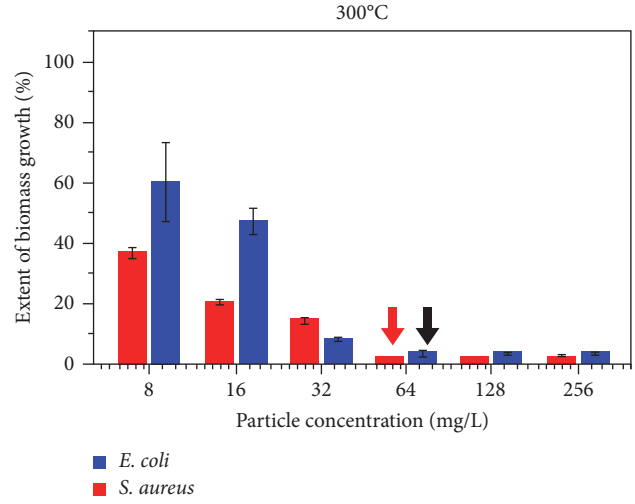

(d)

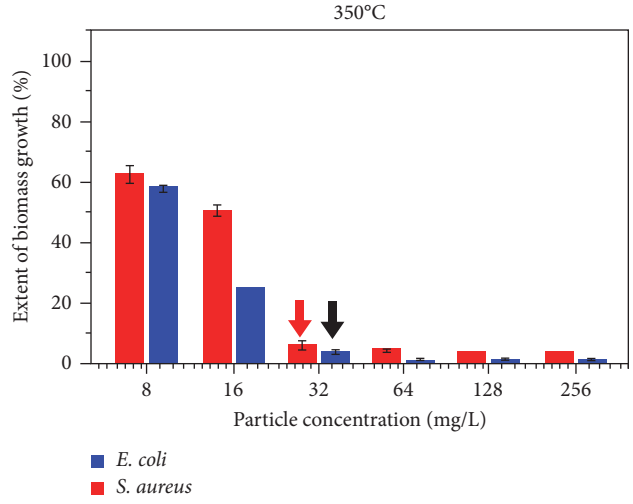

(e)

Temperature (°C)	MIC (mg/L)	
	EC	SA
150	-	-
200	64	64
250	64	64
300	64	64
350	32	32

(f)

Figure 3: Antimicrobial activities of CuO (150°C) and Cu_xP (200–350°C) particles on model bacteria. (a–e) exposure of Gram-positive (*S. aureus*) and Gram-negative (*E. coli*) bacteria to 8–256 mg/L particles at 37°C, 16 hr. The extent of biomass growth was determined relative to cell-only (no particles) control samples. For each of the particle concentration, the experiments were performed with three biological replicates (independent bacterial inocula), each with three technical replicates. (f) The minimum inhibitory concentrations (correspond to ≤5% growth relative to the cell-only control samples) for each of the particle exposure systems.

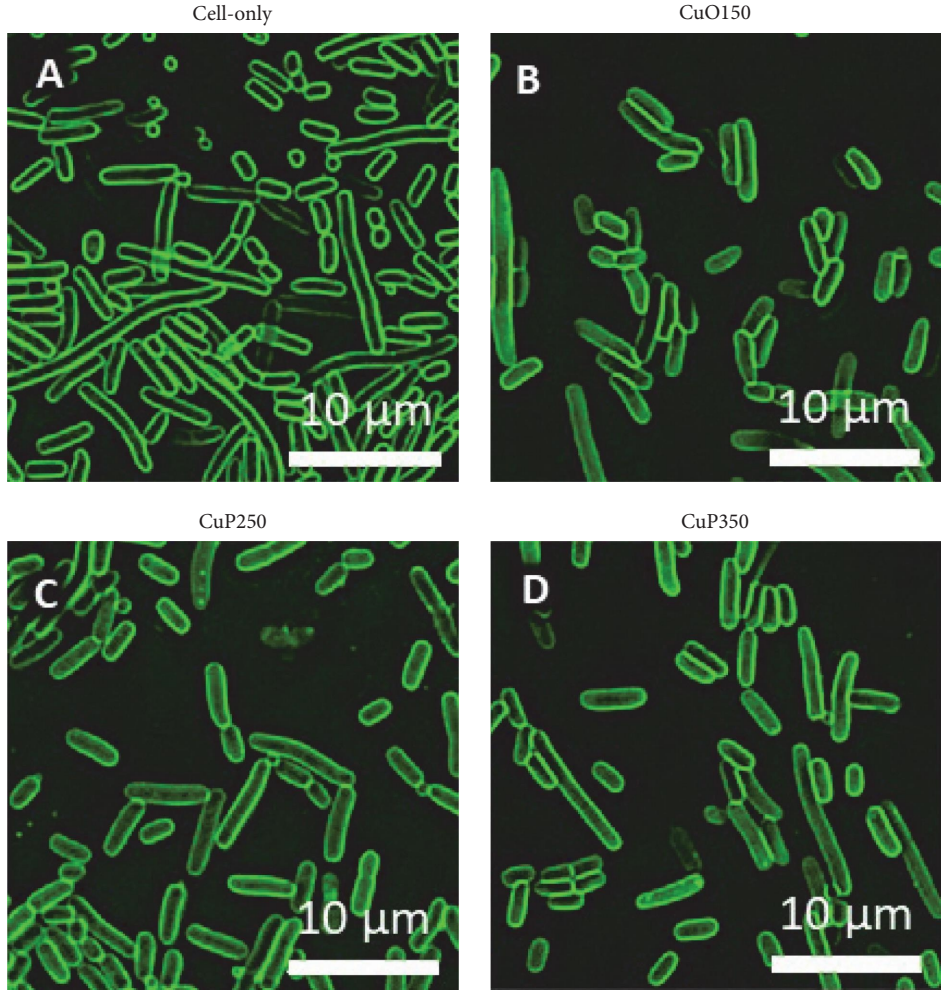

FIGURE 4: Fluorescence micrographs of AM1-43 stained *E. coli* following exposures to CuO and Cu_xP particles. Also shown is the cell-only (no particle) control. The bacteria were exposed to 64 mg/L particle concentration for 1 hr.

compared to the cell-only control. The leaky membrane is also indicated by an influx of the dye into cells, with the evident green fluorescence mass inside the particle-exposed samples, which is absent in the cell-only control [37, 38].

The phospholipid fluorescence staining was also performed on the particle-exposed *S. aureus* samples, however, with inconclusive results (Figure S4). This rather expected observation is likely to result from the presence of relatively thick, outermost peptidoglycan layer in the Gram-positive cell envelope, hence limiting the dye penetrability to reach the inner membrane. Regardless, earlier nanoparticle studies have shown that peptidoglycan is also prone to hydroxyl radical attack [31]. The radical can damage amide bonds that are present in the glycan strands (more specifically, in the amino sugars and peptide moieties) of peptidoglycan. Studies have also indicated hydroxyl radical attack on teichoic acid, another major cell envelope component of Gram-positive bacteria; with the radical targeting the C=O ester, phosphate ester, and amide bonds in the molecule [31]. The known hydroxyl radical targeting on Gram-positive cell envelope components could explain the similar antibacterial activities herein observed between the Gram-positive and Gram-negative models. Taken together, the indicative observations of hydroxyl-radical mediated cell envelope damages, shown with membrane phospholipids in the present work, are in agreement with the growth-inhibiting effects of the CuP350, along with the less potent CuP200, CuP250, and CuP300 particles. The radical is also known to target base pairing in DNA and RNA, as well as introducing covalent modifications in amino acids, such as the sulfur-containing cysteine and methionine, in turn inactivating functional proteins [39–43].

A more detailed investigation revealed other sources for the antibacterial activities, apart from the redox hydroxyl radical generation. This is particularly apparent with the dose-dependent growth inhibition effects seen with the non-hydroxyl radical-producing CuO150 particle (Figure 3(a)). Our leaching studies found that the particle almost completely dissolved (~80% relative to total copper content, measured in MHB culture medium, pH 6), releasing soluble copper into

the exposure systems (Figure S5). The CuO150 is composed of Cu_xO with mainly CuO on its surface (Figure 1). Studies have reported relatively high extent of soluble copper leaching from CuO particles in organic-containing media due to complexation-mediated leaching [29]. Previous work on copper-based particles have established the antibacterial roles of the leached soluble copper, which stimulate oxidative stress in cells, being linked to Cu(II) ion targeting of proteins [29, 43]. A borderline Lewis acid, the ion has high affinities to donor groups in amino acid side chains, such as the $–NH^+$ (in imidazole ring), $–NH_3^+$, and thiol ($–S^-$) groups in histidine, lysine, and cysteine, respectively, forming complexes with the amino acids in proteins [44]. The ion can also disrupt the iron–sulfur (cysteine) clusters that are present in many physiologically essential biosynthetic and catabolic enzymes, releasing the Fenton-active Fe(II) ion, with the latter further reacting with cellular H_2O_2 to form hydroxyl radical [45]. Cu(II) ion has also been indicated to target cell envelopes, disrupting functional groups in peptidoglycan (peptidoglycan is also present in Gram-negative bacteria, as thin layer in between the outer and inner membranes) and phospholipids, the latter affecting membrane permeability [46, 47]. The implied leached soluble Cu-mediated cellular hydroxyl radical generation and cell envelope targeting are consistent with the damaged membrane observation, herein also evident with the CuO150-exposed bacterial samples (Figure 4(b)).

The soluble copper leaching could also contribute to the growth-inhibiting effects of the higher temperature Cu_xP particles. The CuP350 (composed of ∼55% Cu_3P and ∼45% CuP_2, with surface presence of Cu_3P, CuP_2, and $Cu_3(PO_4)_2$, Figure 1) and CuP250 (∼90% Cu_3P and ∼10% CuP_2, with surface presence of mainly Cu_3P and $Cu(OH)_2$, Figure 1) particles had similar extent of soluble copper leaching (∼7% relative to total copper, Figure S5), although much less when compared to CuO150 (∼80% leaching relative to total copper). In addition to the different particle surface composition, the lower leaching could result from the larger aggregate size of the higher temperature Cu_xP particles (Table 1) [5]. Finally, the data also suggest a potential antibacterial contribution from the solid particulates that remain after leaching. This is evident with the CuP300 bacterial exposures, with already ∼40%–60% growth inhibition effects manifesting on both *S. aureus* and *E. coli* at the lowest particle dosage (8 mg/L, Figure 3(d)), despite the only moderate redox hydroxyl radical generation (Figure 2(a)) and leaching of soluble copper (Figure S5). Research inquiries have reported that copper particles can adhere onto bacterial membranes through electrostatic interaction, which leads to membrane damage and in some case, penetration of the particles into the cytoplasm [48–50].

3. Conclusion

Herein, we developed Cu_xP particles for antibacterial purposes, with stable surface presence of Cu(I) species intended for the redox generation of the highly reactive hydroxyl radical. The particles were synthesized via a temperature-dependent phosphorization of $Cu(OH)_2$, with particle surface analysis confirming the stable presence of the Cu(I) state Cu_3P species. The phosphorization process, however, led to sintering effects and increased the particle size. Despite the larger particle size, our studies with Gram-positive and Gram-negative bacteria models showed a significantly higher extent of antimicrobial activities when compared to other copper-based particles. The Cu_xP particles were found to generate hydroxyl radical, most likely involving one-electron reduction of molecular oxygen by the surface Cu(I), leading to the observed inhibition effects on bacterial growth, with further evidence of cell membrane targeting. In summary, the Cu_xP particles with their ability to use molecular oxygen to generate radicals, as well as, apparently, their relatively low extent of copper leaching, present a promising particle technology for alternative antimicrobial applications, in particular for the development of self-disinfecting surfaces, to slow down the fomite transmission of pathogens.

Data Availability

The data used to support the findings of this study are included within the article and supplementary information file.

Conflicts of Interest

The authors declare that they have no conflicts of interest.

Funding

Open access publishing facilitated by University of Technology Sydney, as part of the Wiley - University of Technology Sydney agreement via the Council of Australian University Librarians.

Acknowledgments

The work was supported by the Australian Research Council Discovery Project DP200103587 (Z. Gu) and DP180100474 (C. Gunawan). The authors would also like to acknowledge the use of the facilities within the UNSW Mark Wainwright Analytical Centre and the UoW Electron Microscopy Centre.

Supplementary Materials

Figure S1: Cu 2p XPS spectra of (a) CuO150 and phosphorized Cu_xP: (b) CuP200, (c) CuP250, (d) CuP300, and (e) CuP350. Figure S2: P 2p XPS spectra of (a) CuO150 and phosphorized Cu_xP: (b) CuP200, (c) CuP250, (d) CuP300, and, (e) CuP350. Figure S3: O 1s XPS spectra of (a) CuO150 and phosphorized Cu_xP: (b) CuP200, (c) CuP250, (d) CuP300, and (e) CuP350. Figure S4: Fluorescence micrographs of fluorescent dye (FM4-64) stained *S. aureus* after exposure to Cu_xP particles: (a) Blank, (b) CuO150, (c) CuP250, and (d) CuP350. Figure S5: Solubility of CuO and Cu_xP particles in (a) MHB buffer solution at pH 6 and (b) deionized water. (*Supplementary Materials*)

References

[1] M. L. Ermini and V. Voliani, "Antimicrobial nano-agents: the copper age," *ACS Nano*, vol. 15, no. 4, pp. 6008–6029, 2021.

[2] I. Salah, I. P. Parkin, and E. Allan, "Copper as an antimicrobial agent: recent advances," *RSC Advances*, vol. 11, pp. 18179–18186, 2021.

[3] V. K. Champagne and D. J. Helfritch, "A demonstration of the antimicrobial effectiveness of various copper surfaces," *Journal of Biological Engineering*, vol. 7, Article ID 8, 2013.

[4] H. L. Karlsson, P. Cronholm, Y. Hedberg et al., "Cell membrane damage and protein interaction induced by copper containing nanoparticles—importance of the metal release process," *Toxicology*, vol. 313, no. 1, pp. 59–69, 2013.

[5] G. Applerot, J. Lellouche, A. Lipovsky et al., "Understanding the antibacterial mechanism of CuO nanoparticles: revealing the route of induced oxidative stress," *Small*, vol. 8, no. 21, pp. 3326–3337, 2012.

[6] Z. Wang, N. Li, J. Zhao, J. C. White, P. Qu, and B. Xing, "CuO nanoparticle interaction with human epithelial cells: cellular uptake, location, export, and genotoxicity," *Chemical Research in Toxicology*, vol. 25, no. 7, pp. 1512–1521, 2012.

[7] Y. Shalom, I. Perelshtein, N. Perkas, A. Gedanken, and E. Banin, "Catheters coated with Zn-Doped CuO nanoparticles delay the onset of catheter-associated urinary tract infections," *Nano Research*, vol. 10, pp. 520–533, 2017.

[8] D. Laha, A. Pramanik, A. Laskar, M. Jana, P. Pramanik, and P. Karmakar, "Shape-dependent bactericidal activity of copper oxide nanoparticle mediated by DNA and membrane damage," *Materials Research Bulletin*, vol. 59, pp. 185–191, 2014.

[9] A. Różańska, A. Chmielarczyk, D. Romaniszyn et al., "Antimicrobial properties of selected copper alloys on staphylococcus aureus and *Escherichia coli* in different simulations of environmental conditions: with vs. without organic contamination," *International Journal of Environmental Research and Public Health*, vol. 14, no. 7, Article ID 813, 2017.

[10] J. Zhou, H. Xiang, F. Zabihi, S. Yu, B. Sun, and M. Zhu, "Intriguing antisuperbug Cu_2O@ZrP hybrid nanosheet with enhanced antibacterial performance and weak cytotoxicity," *Nano Research*, vol. 12, pp. 1453–1460, 2019.

[11] J. A. Garza-Cervantes, A. Chávez-Reyes, E. C. Castillo et al., "Synergistic antimicrobial effects of silver/transition-metal combinatorial treatments," *Scientific Reports*, vol. 7, Article ID 903, 2017.

[12] V. V. Tomina, I. M. Furtat, A. P. Lebed et al., "Diverse pathway to obtain antibacterial and antifungal agents based on silica particles functionalized by amino and phenyl groups with Cu(II) ion complexes," *ACS Omega*, vol. 5, no. 25, pp. 15290–15300, 2020.

[13] A. Naz, S. Arun, S. S. Narvi et al., "Cu(II)-carboxymethyl chitosan-silane schiff base complex grafted on nano silica: structural evolution, antibacterial performance and dye degradation ability," *International Journal of Biological Macromolecules*, vol. 110, pp. 215–226, 2018.

[14] S. A. Wilks, H. Michels, and C. W. Keevil, "The survival of *Escherichia coli* O157 on a range of metal surfaces," *International Journal of Food Microbiology*, vol. 105, no. 3, pp. 445–454, 2005.

[15] V. Wonoputri, C. Gunawan, S. Liu et al., "Copper complex in poly(vinyl chloride) as a nitric oxide-generating catalyst for the control of nitrifying bacterial biofilms," *ACS Applied Materials & Interfaces*, vol. 7, no. 40, pp. 22148–22156, 2015.

[16] T. Q. Tran, A. Chinnappan, J. K. Y. Lee et al., "3D printing of highly pure copper," *Metals*, vol. 9, no. 7, Article ID 756, 2019.

[17] J. O. Noyce, H. Michels, and C. W. Keevil, "Potential use of copper surfaces to reduce survival of epidemic meticillin-resistant staphylococcus aureus in the healthcare environment," *Journal of Hospital Infection*, vol. 63, no. 3, pp. 289–297, 2006.

[18] Y. Fujimori, T. Sato, T. Hayata et al., "Novel antiviral characteristics of nanosized copper(I) iodide particles showing inactivation activity against 2009 pandemic H1N1 influenza virus," *Applied and Environmental Microbiology*, vol. 78, no. 4, pp. 951–955, 2012.

[19] N. Shionoiri, T. Sato, Y. Fujimori et al., "Investigation of the antiviral properties of copper iodide nanoparticles against feline calicivirus," *Journal of Bioscience and Bioengineering*, vol. 113, no. 5, pp. 580–586, 2012.

[20] W. Wang, B. Li, H. Yang et al., "Efficient elimination of multidrug-resistant bacteria using copper sulfide nanozymes anchored to graphene oxide nanosheets," *Nano Research*, vol. 13, pp. 2156–2164, 2020.

[21] S. Hussain, E. Aneggi, and D. Goi, "Catalytic activity of metals in heterogeneous fenton-like oxidation of wastewater contaminants: a review," *Environmental Chemistry Letters*, vol. 19, pp. 2405–2424, 2021.

[22] A. V. Kachur, K. D. Held, C. J. Koch, and J. E. Biaglow, "Mechanism of production of hydroxyl radicals in the copper-catalyzed oxidation of dithiothreitol," *Radiation Research*, vol. 147, no. 4, pp. 409–415, 1997.

[23] D. Chao, Q. Dong, J. Chen et al., "Highly efficient disinfection based on multiple enzyme-like activities of Cu_3P nanoparticles: a catalytic approach to impede antibiotic resistance," *Applied Catalysis B: Environmental*, vol. 304, Article ID 121017, 2022.

[24] M. C. Biesinger, "Advanced analysis of copper X-ray photoelectron spectra," *Surface and Interface Analysis*, vol. 49, no. 13, pp. 1325–1334, 2017.

[25] K. Afshinnia and M. Baalousha, "Effect of phosphate buffer on aggregation kinetics of citrate-coated silver nanoparticles induced by monovalent and divalent electrolytes," *Science of The Total Environment*, vol. 581-582, pp. 268–276, 2017.

[26] N. F. D. Vecchia, A. Luchini, A. Napolitano et al., "Tris buffer modulates polydopamine growth, aggregation, and paramagnetic properties," *Langmuir*, vol. 30, no. 32, pp. 9811–9818, 2014.

[27] V. Leandri, J. M. Gardner, and M. Jonsson, "Coumarin as a quantitative probe for hydroxyl radical formation in heterogeneous photocatalysis," *The Journal of Physical Chemistry C*, vol. 123, no. 11, pp. 6667–6674, 2019.

[28] S. Sharma and K. Kumar, "Aloe-vera leaf extract as a green agent for the synthesis of CuO nanoparticles inactivating bacterial pathogens and dye," *Journal of Dispersion Science and Technology*, vol. 42, no. 13, pp. 1950–1962, 2021.

[29] C. Gunawan, W. Y. Teoh, C. P. Marquis, and R. Amal, "Cytotoxic origin of copper(II) oxide nanoparticles: comparative studies with micron-sized particles, leachate, and metal salts," *ACS Nano*, vol. 5, no. 9, pp. 7214–7225, 2011.

[30] L. Argueta-Figueroa, R. A. Morales-Luckie, R. J. Scougall-Vilchis, and O. F. Olea-Mejía, "Synthesis, characterization and antibacterial activity of copper, nickel and bimetallic Cu–Ni nanoparticles for potential use in dental materials," *Progress in Natural Science: Materials International*, vol. 24, no. 4, pp. 321–328, 2014.

[31] C. Gunawan, M. B. Faiz, R. Mann et al., "Nanosilver targets the bacterial cell envelope: the link with generation of reactive oxygen radicals," *ACS Applied Materials & Interfaces*, vol. 12, no. 5, pp. 5557–5568, 2020.

[32] A. Samunl and P. Neta, "Electron spin resonance study of the reaction of hydroxyl radicals with pyrrole, imidazole, and related compounds," *The Journal of Physical Chemistry*, vol. 77, no. 13, pp. 1629–1635, 1973.

[33] H. Yin, L. Xu, and N. A. Porter, "Free radical lipid peroxidation: mechanisms and analysis," *Chemical Reviews*, vol. 111, no. 10, pp. 5944–5972, 2011.

[34] R. Hong, T. Y. Kang, C. A. Michels, and N. Gadura, "Membrane lipid peroxidation in copper alloy-mediated contact killing of *Escherichia coli*," *Applied and Environmental Microbiology*, vol. 78, no. 6, pp. 1776–1784, 2012.

[35] I. Fishov and C. L. Woldringh, "Visualization of membrane domains in *Escherichia coli*," *Molecular Microbiology*, vol. 32, no. 6, pp. 1166–1172, 1999.

[36] J. R. Zupan, T. A. Cameron, J. Anderson-Furgeson, and P. C. Zambryski, "Dynamic FtsA and FtsZ localization and outer membrane alterations during polar growth and cell division in *Agrobacterium tumefaciens*," *Proceedings of the National Academy of Sciences*, vol. 110, no. 22, pp. 9060–9065, 2013.

[37] L. R. Griffing, "FRET analysis of transmembrane flipping of FM4–64 in plant cells: is FM4–64 a robust marker for endocytosis?" *Journal of Microscopy*, vol. 231, no. 2, pp. 291–298, 2008.

[38] J. Derk Te Winkel, D. A. Gray, K. H. Seistrup, L. W. Hamoen, and H. Strahl, "Analysis of antimicrobial-triggered membrane depolarization using voltage sensitive dyes," *Frontiers in Cell and Developmental Biology*, vol. 4, Article ID 29, 2016.

[39] S. B. Nimse and D. Pal, "Free radicals, natural antioxidants, and their reaction mechanisms," *RSC Advances*, vol. 5, pp. 27986–28006, 2015.

[40] M. A. Kohanski, D. J. Dwyer, B. Hayete, C. A. Lawrence, and J. J. Collins, "A common mechanism of cellular death induced by bactericidal antibiotics," *Cell*, vol. 130, no. 5, pp. 797–810, 2007.

[41] B. Ezraty, A. Gennaris, F. Barras, and J.-F. Collet, "Oxidative stress, protein damage and repair in bacteria," *Nature Reviews Microbiology*, vol. 15, pp. 385–396, 2017.

[42] B. D'Autréaux and M. B. Toledano, "ROS as signalling molecules: mechanisms that generate specificity in ROS homeostasis," *Nature Reviews Molecular Cell Biology*, vol. 8, pp. 813–824, 2007.

[43] G. Guan, L. Zhang, J. Zhu, H. Wu, W. Li, and Q. Sun, "Antibacterial properties and mechanism of biopolymer-based films functionalized by CuO/ZnO nanoparticles against *Escherichia coli* and *Staphylococcus aureus*," *Journal of Hazardous Materials*, vol. 402, Article ID 123542, 2021.

[44] R. Osterberg and B. Sjoberg, "Copper(I) and Copper(II) complexes in solution and the crystalline state," *Journal of The American Oil Chemists Society*, vol. 48, no. 10, pp. 525-526, 1971.

[45] E. Valentin, A. L. Bottomley, G. S. Chilambi et al., "Heritable nanosilver resistance in priority pathogen: a unique genetic adaptation and comparison with ionic silver and antibiotics," *Nanoscale*, vol. 12, pp. 2384–2392, 2020.

[46] T. Ishida, "Bacteriolyses of bacterial cell walls by Cu(II) and Zn(II) ions based on antibacterial results of dilution medium method and halo antibacterial test," *Journal of Advanced Research in Biotechnology*, vol. 2, no. 2, pp. 1–12, 2017.

[47] Z. Liu, J. Ye, A. Rauf et al., "A flexible fibrous membrane based on copper(ii) metal–organic framework/poly(lactic acid) composites with superior antibacterial performance," *Biomaterials Science*, vol. 9, pp. 3851–3859, 2021.

[48] A. Thill, O. Zeyons, O. Spalla et al., "Cytotoxicity of CeO_2 nanoparticles for *Escherichia coli*. physico-chemical insight of the cytotoxicity mechanism," *Environmental Science & Technology*, vol. 40, no. 19, pp. 6151–6156, 2006.

[49] J. S. McQuillan, H. G. Infante, E. Stokes, and A. M. Shaw, "Silver nanoparticle enhanced silver ion stress response in *Escherichia coli* K12," *Nanotoxicology*, vol. 6, no. 8, pp. 857–866, 2012.

[50] Y.-N. Chang, M. Zhang, L. Xia, J. Zhang, and G. Xing, "The toxic effects and mechanisms of CuO and ZnO nanoparticles," *Materials*, vol. 5, no. 12, pp. 2850–2871, 2012.